Organic Electronics 13 (2012) 1171–1177

Contents lists available at SciVerse ScienceDirect

Organic Electronics

journal homepage: www.elsevier.com/locate/orgel

Effects of ZnO fabricating process on the performance of inverted organic solar cells

Jia Hu, Zhongwei Wu, Huaixin Wei, Tao Song, Baoquan Sun *

Jiangsu Key Laboratory for Carbon-Based Functional Materials & Devices, Institute of Functional Nano & Soft Materials (FUNSOM), Soochow University, 199 Ren'ai Road, Suzhou 215123, PR China

ARTICLE INFO

Article history:
Received 14 January 2012
Received in revised form 27 February 2012
Accepted 17 March 2012
Available online 7 April 2012

Keywords:
Zinc oxide
Inverted solar cell
Morphology
Charge extraction
Work function

ABSTRACT

The effects of zinc oxide (ZnO) fabricating process on the performance of the inverted bulk heterojunction (BHJ) solar cells were explored in this study. The ZnO layers were prepared by either sputtering or solution-processed method. These ZnO films on the indium tin oxide (ITO) substrates were used as the cathode of the inverted solar cells. It was found that the topography of the ZnO films played a leading role on the device performance. The devices based on solution-processed ZnO films displayed better electric output compared with that of sputtered ones. The measurement of capacitance against bias voltage indicated that ZnO film with certain degree of roughness exhibited high charge extraction efficiency, which resulted in improved device performance. The measurement of ultraviolet photoelectron spectroscopy revealed that a shift of work function was observed due to the fabricating process of ZnO films.

1. Introduction

In recent years, great efforts have been made to improve the performance of the organic bulk-heterojunction (BHJ) solar cells [1–3]. The BHJ structure provided a facial approach to fabricate devices with high performance. Conventional BHJ solar cells were fabricated with a transparent conductive anode (e.g. indium tin oxide, ITO) and a low-work-function metal cathode (e.g. Al) to collect holes and electrons, respectively. Normally, a hole conducting layer of poly(3,4-ethylenedioxythiophene)/poly(styrene sulfonate) (PEDOT:PSS) was deposited onto the ITO substrate to enhance the collection efficiency of holes as well as smoothing the roughness of ITO. However, a drawback of instability was accompanied simultaneously due to the gradual etching of ITO if directly contacted with PEDOT:PSS [4]. In addition, the low-work-function cathode was susceptible to degradation by oxygen and moisture, which deteriorated the device performance [5,6]. In order to overcome these problems, inverted device architecture, in which the positions of the anode and cathode were reversed, was employed [7,8]. In this structure, a layer of PEDOT:PSS or high-work-function transition metal oxide (e.g. V_2O_5, MoO_x) was deposited onto the active layer acting as hole-collecting layer before the evaporation of the relatively nonreactive electron collection layer (e.g. Ag, Au) [6,9]. In addition, the high-work-function transition metal oxide could also act as electron-blocking layer. This approach alleviated the device instability problem and enhanced the device performance effectively [2,7].

Although dramatic improvement of stability has been obtained by using inverted structure, many challenges still remained. Typically, the inverted BHJ solar cells exhibited inferior performance compared with the conventional ones. Inserting an electron collection layer of metal oxide (e.g. ZnO, TiO_2, Al_2O_3, PbO) between active layer and cathode could alleviate this problem [10–14]. In addition, cesium carbonate (Cs_2CO_3) and polyethylene oxide (PEO) have also been used to modify the ITO substrate to enhance the electronic performance of devices [15,7,16].

Among the documented electron collection materials, ZnO was one of the most widely explored due to its high

* Corresponding author. Tel.: +86 512 6588 0951.
E-mail address: bqsun@suda.edu.cn (B. Sun).

1566-1199/$ - see front matter © 2012 Elsevier B.V. All rights reserved.
http://dx.doi.org/10.1016/j.orgel.2012.03.021

mobility, stability, as well as the non-toxic nature [17–21]. Solution-processed ZnO nanocrystals (nc-ZnO) have been extensively used for the inverted device applications. Although various ZnO fabrication methods were explored, limited knowledge on the effects of ZnO fabricating process on the performance of inverted solar cells has been disclosed so far [22–26]. In this manuscript, a series of ZnO films prepared by various processing methods were fabricated to explore the device performance affected by the processing steps. The results indicated that the topography of ZnO film as well as its work function played a critical role on the device performance, which could be ascribed to the charge extraction efficiency in these structures.

2. Experimental

2.1. ZnO synthesis

Nc-ZnO were synthesized by hydrolysis hydroxide at a low temperature [24,26]. In brief, 4.46 mmol zinc acetate dihydrate was dissolved in methanol at room temperature, after being magnetic stirred to 60 °C, 7.22 mmol potassium hydroxide in methanol was dropped into zinc acetate solution within 15 min. The resulted mixture was then stirred at 60 °C for 120 min to obtain nanocrystals with a diameter of approximate 6 nm. After washing steps, the nanocrystals were dispersed in chloroform with a concentration of 80 mg/mL. And the additional solution, namely zinc precursor solution, was prepared using 0.05 M zinc acetate dihydrate and 0.05 methanolamine in ethylene glycol monomethyl ether [27]. The zinc precursor solution was stirred for 12 h at room temperature before being deposited onto the pre-spin-coated nc-ZnO layers.

2.2. ZnO film fabrication

ZnO films were mainly fabricated in three different ways: ZnO film prepared by the radio-frequency (RF) magnetic sputtering method, ZnO film made by the spin-coating method from an nc-ZnO solution and ZnO film fabricated by the spin-coating method from using a zinc precursor solution onto pre-spin-coated nc-ZnO film. Here, the fabrication processes of these three kinds of ZnO films would be detailed. In the sputtering process, a constant RF power of 100 W, an airflow rate of 3 cm^3/min and working pressure of 10 mPa were used [22]. No further post-treatment was utilized for the sputtered ZnO film. And for the bare nc-ZnO films, nc-ZnO solutions with concentrations of 2 mg/mL, 6 mg/mL, 12 mg/mL, 15 mg/mL and 18 mg/mL were used to fabricate the films, respectively. The spin rate was 2500 rpm for 1 min. The films were then annealed in ambient at 270 °C for 20 min. For the films modified with zinc precursor solution, the substrate ZnO layers were prepared just using the aforementioned nc-ZnO solutions and annealed at 270 °C too. With a spin speed of 2500 rpm and a spin time of 1 min, the zinc precursor was then spin-coated onto the as-prepared ZnO films. The films were further baked at 200 °C in ambient for 20 min. During the annealing process, the zinc precursor was decomposed into ZnO, which increased the surface roughness of as-prepared ZnO film. In addition, the precursor layer could fill in the inter-particle space.

2.3. Device fabrication

The schematics cross-section of the inverted BHJ solar cells was depicted in Fig. 1. ITO coated glasses (10 Ω/sq) were ultrasonicated in de-ionized water, acetone and ethanol, and then treated with UV-ozone for 15 min. ZnO films were coated onto the ITO coated glasses with aforementioned three methods. The active layer was sandwiched between the bottom cathode ZnO (ITO) and the positive electrode MoO_x (Ag). Without any further purification treatment, the poly(3-hexylthiopene) (P3HT) and [6,6]-phenyl-C_{61}-butyric acid methyl esters (PCBM) (1:1, 15 mg/mL) in 1,2-dichlorobenzene were spin-coated onto the top of ZnO layers in a N_2 ambient, and annealed at 150 °C for 30 min subsequently [28,29]. Hole transporting layer MoO_x and Ag electrode were then deposited in sequence. The effective area of the devices was restricted to 0.04 cm^2 by using a shadow mask when depositing MoO_x layer and Ag anode.

2.4. Characterization and testing

The current density versus voltage (*J*–*V*) characteristics of the devices were characterized by a Keithley 2612 source measurement unit. A Newport 91160 solar simulator with a xenon lamp (300 W) coupled with an air mass (AM) 1.5 filter was used as the light source. Newport monochromator 74125 and power meter 1918 with silicon detector 918D were used in the external quantum efficiency (EQE) measurements. The capacitance versus voltage (*C*–*V*) measurement was carried out using Wayne Kerr 6500B impedance analyzer. A 50% filter was used in company with a 450 nm cut-off filter during the *C*–*V* measurement under irradiation. Ultraviolet photoelectron spectroscopy (UPS) measurements were performed in a

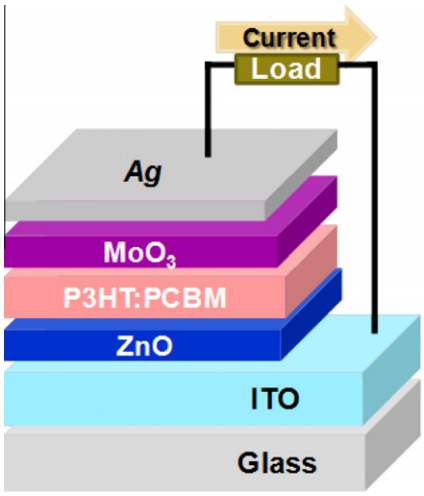

Fig. 1. The scheme of the inverted structural BHJ solar cell with ZnO as the electron selective layer.

KRATOS ULTRA-DLD ultrahigh vacuum surface analysis system. The spectra were measured by using an unfiltered HeI (21.22 eV) gas discharge lamp and a total instrumental energy resolution of 100 meV.

3. Results and Discussion

3.1. ZnO fabrication method

In order to explore the effects of ZnO films on the performance of inverted BHJ solar cells, ZnO films fabricated by different methods were utilized as electron accepting layer. Three kinds of ZnO films were investigated. Traditionally, ZnO film could be easily prepared by RF sputtering method with good electronic characters [22]. Fig. 2(a) showed the performance of the device made from the sputtered ZnO film. The device with the open circuit voltage (V_{oc}) of 0.60 V, the short current density (J_{sc}) of 8.22 mA/cm^2, and the fill fact (FF) of 0.383, yielded the power conversion efficiency (PCE) of 1.9%.

Whereas, the devices made from solution processed ZnO films showed improved performance with respect to those from sputtered ones. The device with the V_{oc} of 0.55 V, the J_{sc} of 8.77 mA/cm^2, the FF of 0.566, yielded the PCE of 2.8% (Fig. 2(b)). Further enhancement was achieved via modifying with zinc precursor, as Fig. 2(c). The device with the V_{oc} of 0.57 V, the J_{sc} of 10.62 mA/cm^2, the FF of 0.59, achieved the PCE of 3.6%. The addition of zinc precursor solution onto the nc-ZnO films dramatically improved the devices performance. The device performances of these three kinds of devices described above were listed in Table 1.

3.2. nc-ZnO concentration

Since dramatic enhancement of device performance has been observed when using zinc precursor modified ZnO films, different concentrations of nc-ZnO solutions in the following set of experiments were utilized to investigate the influence of nc-ZnO concentration on the performance. PCE, FF, J_{sc}, and V_{oc} of BHJ cells made from various concentrations of nc-ZnO solutions were summarized as a function of concentration in Fig. 3. The nc-ZnO solutions with the concentration of 2 mg/mL, 6 mg/mL, 12 mg/mL, 15 mg/mL and 18 mg/mL were used in this set of experiments. The corresponding electronic properties were summarized in Table 2. The higher the concentration of nc-ZnO solution was, the better the device performance was. When the device was fabricated from the 15 mg/mL nc-ZnO solution, a significant 40.9% increase in PCE, a 13.9% increase in FF and a 25.2% increase in J_{sc} were obtained with respect to that from the 12 mg/mL solution. However, no further increase of device performance was obtained at the higher concentration of the nc-ZnO solution (>15 mg/mL). The nc-ZnO solution with 15 mg/mL was found to be optimal, as shown in Fig. 3(d). The EQE spectra (Fig. 4(d)) also reached the highest value of 60% at the absorption peak of P3HT.

Table 1
Parameters extracted from the *J–V* curves (Fig. 2) of devices using (a) sputtered ZnO, (b) spin-coating 15 mg/mL nc-ZnO solution without zinc precursor, and (c) spin-coating 15 mg/mL nc-ZnO solution and zinc precursor.

Device	V_{oc} (V)	J_{sc} (mA/cm^2)	FF	PCE (%)
a	0.60	8.22	0.383	1.9
b	0.55	8.77	0.566	2.8
c	0.57	10.62	0.590	3.6

3.3. Roughness of ZnO film

As shown in the *J–V* curves (Figs. 2 and 3), the performance of our devices was remarkably enhanced by the inserting of the precursor solution. Furthermore, utilization of different concentrations of nc-ZnO solutions resulted in dramatically variation of device performance. To figure out the origin of the effects, atomic force microscope (AFM) images with taping mode were taken to verify the morphology of these ZnO films. Fig. 5 revealed the surface topography of ZnO films fabricated by the method of RF sputtering, the method of spin-coating 15 mg/mL nc-ZnO solution and the method of spin-coating nc-ZnO films with additional precursor solution insertion. The corresponding root-mean-square (RMS) roughness values were 0.95 nm, 2.61 nm and 3.59 nm. As for BHJ solar cells, the coarse

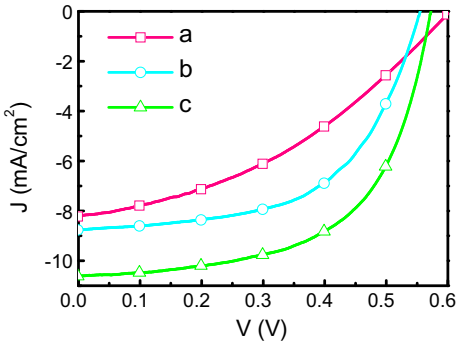

Fig. 2. *J–V* characteristic curves of devices based on ZnO film fabricated by (a) sputtered ZnO, (b) spin-coating 15 mg/mL nc-ZnO solution without zinc precursor, (c) spin-coating 15 mg/mL nc-ZnO solution and zinc precursor.

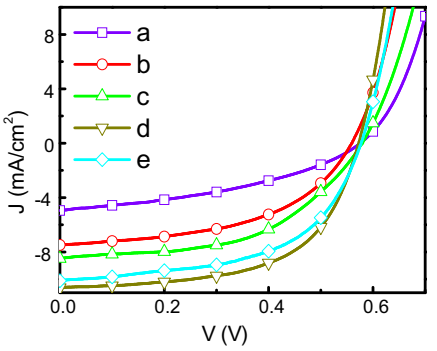

Fig. 3. *J–V* curves of the devices based on ZnO film fabricated by spin-coating (a) 2 mg/mL, (b) 6 mg/mL, (c) 12 mg/mL, (d) 15 mg/mL, and (e) 18 mg/mL nc-ZnO solutions and zinc precursor.

Table 2
Parameters extracted from the *J*–*V* curves (Fig. 3) of devices based on ZnO film fabricated by spin-coating (a) 2 mg/mL, (b) 6 mg/mL, (c) 12 mg/mL, (d) 15 mg/mL, and (e) 18 mg/mL nc-ZnO solutions and zinc precursor.

Device	V_{oc} (V)	J_{sc} (mA/cm^2)	FF (%)	PCE (%)
a	0.58	4.94	39.6	1.1
b	0.56	7.48	50.3	2.1
c	0.58	8.48	51.8	2.5
d	0.57	10.62	59.0	3.6
e	0.58	10.12	55.1	3.2

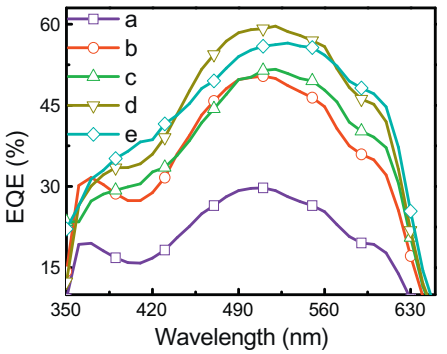

Fig. 4. The EQE spectra of the devices based on ZnO film fabricated by spin-coating (a) 2 mg/mL, (b) 6 mg/mL, (c) 12 mg/mL, (d) 15 mg/mL, and (e) 18 mg/mL nc-ZnO solutions and zinc precursor.

morphology of the films enlarged the interface area of ZnO, providing an intimate intermixing for efficient exciton dissociation, which was beneficial to devices performance [30–32]. This perspective was well supported by the surface roughness values of these three films. The increased roughness enlarged the interface area between ZnO film and the active layer, leading to the enhancement of charge collection efficiency.

AFM measurements were also taken to study the dependence of photovoltaic performance on the nc-ZnO solution concentrations. Fig. 6 illustrated the AFM images of the films using zinc precursor based on different concentrations of nc-ZnO solutions. The RMS roughness values of the ZnO films consistently grew with increasing the concentration of nc-ZnO solutions, generating a RMS value difference of only 2.14 nm from the film made by 2 mg/mL to that by 15 mg/mL. Nevertheless, the RMS value dramatically jumped from 3.59 nm (from 15 mg/mL) to 9.18 nm (from 18 mg/mL). Simultaneously, the corresponding device made from the 15 mg/mL nc-ZnO solution reached the peak PCE. Further increase of the concentration of nc-ZnO solution accompanying with higher rough surface led to the deterioration of PCE. It was noted that, the drop of PCE originated from the diminishing FF, which might be associated with inefficient charge extraction. If the ZnO film became too rough to be tolerated for forming a uniform layer on the top of active layer, it would be rather difficult to cover the P3HT:PCBM layer uniformly with MoO_x and Ag by the thermal evaporation. The vacuum deposition film could be dramatically affected by "shadow effect" (Fig. S1) [33]. The non-continuous anode would lead to inefficient charge extraction. The separated charge carriers

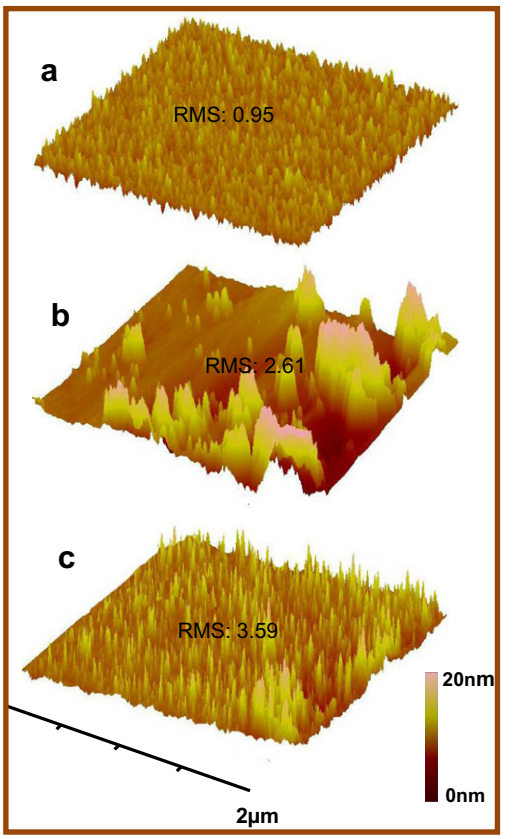

Fig. 5. AFM surface images (2 μm × 2 μm) of ZnO films fabricated by (a) sputtering ZnO, the method of (b) spin-coating 15 mg/mL nc-ZnO solution without zinc precusor, the method of (c) spin-coating zinc precursor onto the pre-spin-coated nc-ZnO film.

could recombine again if they were not promptly collected by the electrodes. In combination of the two effects, the total PCE would decrease when the morphology of ZnO film was too rough to form a continuous electrode.

3.4. Charge extraction

The variation of device performance especially the solution processed ones was explored by capacitance-voltage (*C*–*V*) measurements [34,35]. The *C*–*V* measurements were carried out under either AM 1.5 irradiation with a 450 nm cut-off filter or dark at the room temperature. The capacitance was measured against different bias voltages, with AC excitation amplitude of 200 mV at frequency of 1 kHz. The capacitance was defined by $C = \varepsilon A/d = Q/V$, where A was the junction area, ε was permittivity and d was the separation between positive plate and negative plate, Q was the charges accumulated on the positive and negative plates, V was the applied voltage. The capacitance here was plotted per unit base-area (the flat area of capacitance which was equal to the device area) instead of junction-area (the actually device area counting in the surface roughness). Driven by the forward electric field between anode and cathode, the values of the capacitance under dark offered a perspective to evaluate the area of heterojunction ($C = \varepsilon A/d$). The

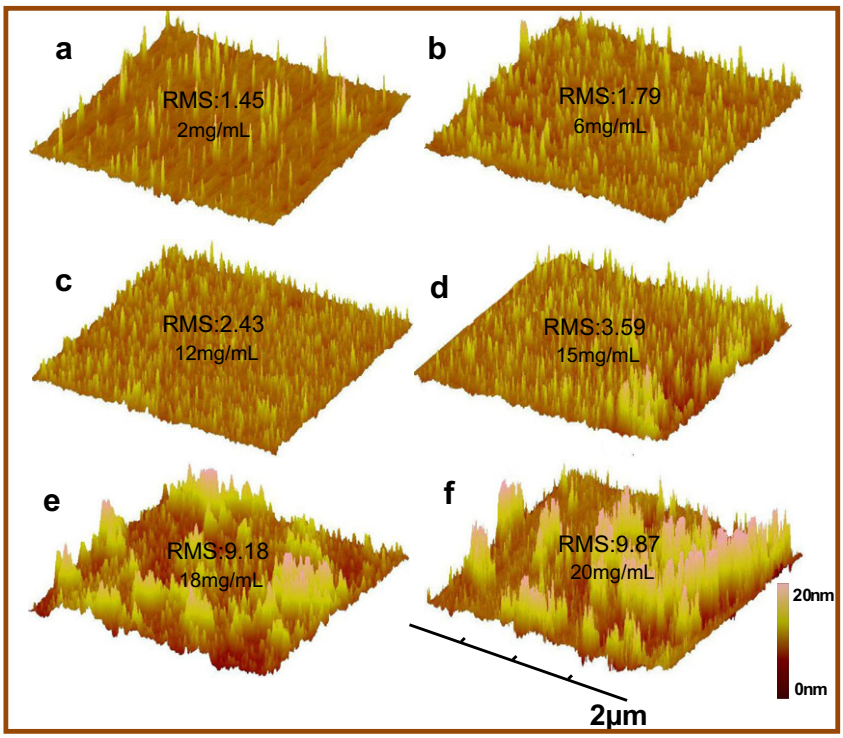

Fig. 6. AFM surface images (2 μm × 2 μm) of ZnO films fabricated by spin-coating (a) 2 mg/mL, (b) 6 mg/mL, (c) 12 mg/mL, (d) 15 mg/mL, (e) 18 mg/mL, and (f) 20 mg/mL nc-ZnO solutions and zinc precursor.

corresponding maximum values of capacitance in dark, which displayed 146.29 $nFcm^{-2}$, 157.85 $nFcm^{-2}$ and 136.79 $nFcm^{-2}$, were of the zinc precursor modified devices using 15 mg/mL (Fig. 7(a)) and 20 mg/mL (Fig. 7(b)) nc-ZnO solutions, and the device just using 15 mg/mL nc-ZnO (Fig. 7(c)). The enlarged interface area due to the coarse morphology was proved directly by the results of the capacitance in dark. For the aforementioned three devices, the maximum capacitance values under dark were consistent with that of the RMS roughness values of these ZnO films.

In the operation process of photovoltaic devices, photogenerated carriers would be transported to the corresponding electrodes upon irradiation. The difference of the capacitance values between dark and irradiating conditions could be a lateral evidence to evaluate the ability of devices to effectively drive carriers to minimize the charge accumulation. The charges accumulated in the electrodes were proportional to the value of capacitance difference ($Q = C^*V$) [36]. In this regard, with the difference peak capacitance values of 37.5 nF/cm^2 (Fig. 7(a) 15 mg/mL with precursor) and 50.7 nF/cm^2 (Fig. 7(c) 15 mg/mL without precursor), the device modified with zinc precursor would indicate better electron extraction efficiency compared with devices barely using nc-ZnO. However, over-coarse morphology of ZnO film brought about no benefits to charge extraction, which was supported by the *C–V* curves in Fig. 7b. The difference peak capacitance value of device (Fig. 7(b)) reached 49.6 nF/cm^2, which was much larger than that of device Fig. 7(a). The over-coarse ZnO film did possess large interface for charge generation while accompanying with drawback of charge extraction. It provided a unique evidence that the morphology played a critical role on the inverted BHJ devices. Two cartoons were drawn to elucidate the effects of the charge accumulation caused by the coarse morphology, as shown in Fig. 8. The smooth morphology of ZnO film provided few interface area for charge generation and extraction, leading to the poor performance of device directly. Whereas, charge accumulation in the interface would be increased due to the un-continuous electrode caused by the "shadow effect".

3.5. UPS measurement

Ultraviolet photoelectron spectroscopy (UPS) analysis was performed to explore the shift of work function due to the fabricating process of ZnO films. It has been reported that the energy level offsets played a crucial role in determining charge generation and transport processes in OPVs [37,38]. The work functions of the ZnO films could be evaluated by subtracting the cutoff value from the excitation source of 21.2 eV. The work functions of 4.21, 3.99, and 4.16 eV for the films fabricated by (a) sputtering method, (b) spin-coating 15 mg/mL nc-ZnO solution, and (c) spin-coating zinc precursor onto the pre-spin-coated 15 mg/mL nc-ZnO film were obtained, respectively. It was found that the sputtered ZnO film displayed the highest work function value, shown in the right spectrum (Fig. 9(a)). In combination with the inferior morphology of sputtered ZnO, the high-work-function sputtered ZnO film did not achieve the highest devices. Device made from

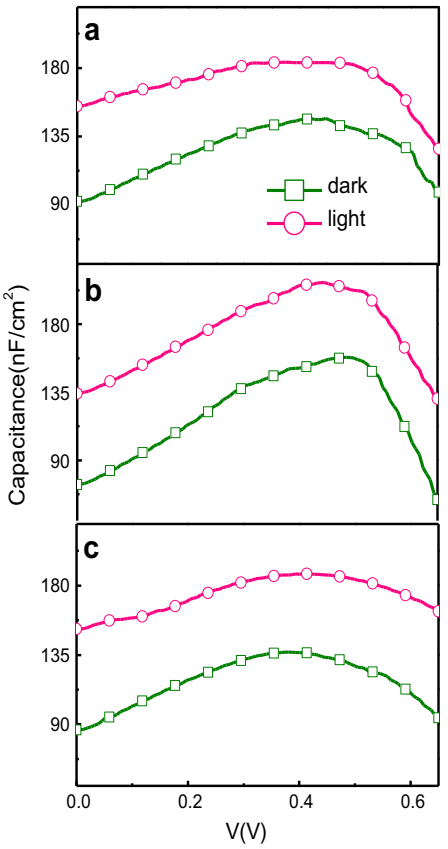

Fig. 7. *C–V* characteristics of devices under either AM 1.5 irradiation with a 450 nm cut-off filter or dark at room temperature, the corresponding devices were devices based on ZnO film fabricated by spin-coating (a) 15 mg/mL and zinc precursor, (b) 20 mg/mL nc-ZnO solutions and zinc precursor, and (c) 15 mg/mL nc-ZnO solution without zinc precursor.

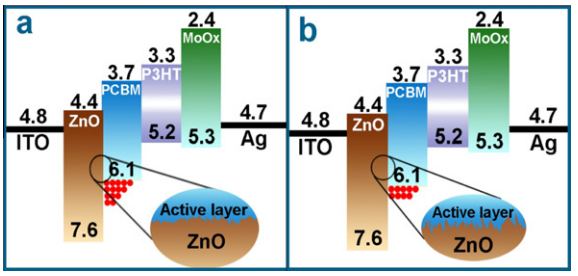

Fig. 8. Energetic configuration of inverted BHJ device, which included a schematic illustration of trap density in the interface of active layer and electrode. Red circles represented the density of charges accumulated in the interface. The coarser morphology of ZnO film enlarged the efficient charge extraction area, relieving the charge accumulation in the interface, which could be vividly illustrated by the number of red circles in Fig. 8(b). The unit was eV, and the corresponding devices were ones using (a) smooth surface topography ZnO film and (b) relatively rough morphology ZnO film.

nc-ZnO was of the lowest work function (Fig. 9(b)). Nonetheless, the inferior device performance in Fig. 2(a) was not consistent with the preferably work function value of the bare nc-ZnO device. In spite of the low work function of

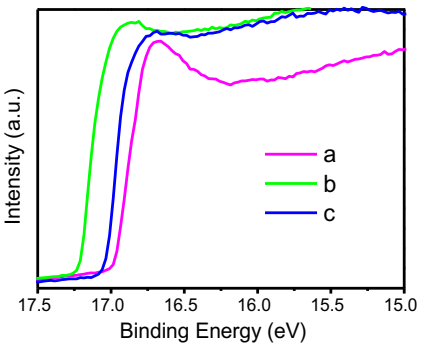

Fig. 9. The UPS spectra of ZnO films on ITO substrates have been included for comparison: (a) film made by sputtering method, (b) film fabricated by spin-coating 15 mg/mL nc-ZnO solution, and (c) film fabricated by spin-coating zinc precursor onto the pre-spin-coated 15 mg/mL nc-ZnO film.

the bare nc-ZnO film, the film was too smooth to afford sufficient exciton dissociation areas, leading to the poor device performance. Hence, the device performance was the combination effects related with morphology as well as work function.

4. Conclusion

In summary, fabricating procedure of ZnO film played a critical role on the performance of inverted BHJ solar cell. Diverse morphology of ZnO films was obtained via different fabrication methods, leading to dramatically difference of the device performance. The topography and work function of ZnO film played a leading role on the device performance. The ZnO film with proper coarse surface morphology provided large interface for charge generation, and it was verified by capacitance measurement. However, the device performance would be deteriorated due to inefficient charge extraction. The UPS spectra showed that the ZnO fabricating process did have effect on the work function of ZnO films, resulting in variation of device performance accordingly. In a word, both morphology and work function of ZnO was dominated factors on the performance of inverted BHJ device.

Acknowledgments

This work was supported by the National Basic Research Program of China (973 Program) (Grant No. 2012CB932402), National Natural Science Foundation of China (Grant Nos. 91123005, 60976050, and 61176057), the Natural Science Foundation of Jiangsu Province (BK2010003), the Priority Academic Program Development of Jiangsu Higher Education Institutions.

Appendix A. Supplementary data

Supplementary data associated with this article can be found, in the online version, at http://dx.doi.org/10.1016/j.orgel.2012.03.021.

References

[1] C.J. Brabec, S. Gowrisanker, J.J.M. Halls, D. Laird, S.J. Jia, S.P. Williams, Adv. Mater. 22 (2010) 3839.
[2] F. Zhang, X. Xu, W. Tang, J. Zhang, Z. Zhuo, J. Wang, J. Wang, Z. Xu, Y. Wang, Sol. Energy Mater. Sol. Cells 95 (2011) 1785.
[3] B.C. Thompson, J.M.J. Fréchet, Angew. Chem. Int. Ed. 47 (2008) 58.
[4] M.P.D. Jong, L.J.V. IJzendoorn, M.J.A.D. Voigt, Appl. Phys. Lett. 77 (2000) 2255.
[5] M. Lira-Cantu, K. Norrman, J.W. Andreasen, F.C. Krebs, Chem. Mater. 18 (2006) 5684.
[6] Y. Şahin, S. Alem, R. de Bettignies, J.-M. Nunzi, Thin Solid Films 476 (2005) 340.
[7] G. Li, C.-W. Chu, V. Shrotriya, J. Huang, Y. Yang, Appl. Phys. Lett. 88 (2006) 253503.
[8] C.H. Hsieh, Y.J. Cheng, P.J. Li, C.H. Chen, M. Dubosc, R.M. Liang, C.S. Hsu, J. Am. Chem. Soc. 132 (2010) 4887.
[9] A.K.K. Kyaw, X.W. Sun, C.Y. Jiang, G.Q. Lo, D.W. Zhao, D.L. Kwong, Thin Solid Films 93 (2008) 221107.
[10] C.-Y. Li, T.-C. Wen, T.-H. Lee, T.-F. Guo, J.-C.-A. Huang, Y.-C. Lin, Y.-J. Hsu, J. Mater. Chem. 19 (2009) 1643.
[11] C. Waldauf, M. Morana, P. Denk, P. Schilinsky, K. Coakley, S.A. Choulis, C.J. Brabec, Appl. Phys. Lett. 89 (2006) 233517.
[12] Y. Zhou, H. Cheun, J.W.J. Potscavage, C. Fuentes-Hernandez, S.-J. Kim, B. Kippelen, J. Mater. Chem. 20 (2010) 6189.
[13] H. Zhang, J. Ouyang, Appl. Phys. Lett. 97 (2010) 063509.
[14] H. Zhang, J. Ouyang, Org. Electron. 12 (2011) 1864.
[15] Y.-I. Lee, J.-H. Youn, M.-S. Ryu, J. Kim, H.-T. Moon, J. Jang, Org. Electron. 12 (2011) 353.
[16] Y. Zhou, F. Li, S. Barrau, W. Tian, O. Inganäs, F. Zhang, Sol. Energy Mater. Sol. Cells 93 (2009) 497.
[17] M. Lira-Cantu, F.C. Krebs, Sol. Energy Mater. Sol. Cells 90 (2006) 2076.
[18] Y. Liu, M.A. Summers, C. Edder, J.M.J. Fréchet, M.D. McGehee, Adv. Mater. 17 (2005) 2960.
[19] S.K. Hau, H.-L. Yip, N.S. Baek, J. Zou, K. O'Malley, A.K.-Y. Jen, Appl. Phys. Lett. 92 (2008) 253301.
[20] J. Huang, Z. Yin, Q. Zheng, Energy Environ. Sci. 4 (2011) 3861.
[21] S. Park, S.J. Tark, J.S. Lee, H. Lim, D. Kim, Sol. Energy Mater. Sol. Cells 93 (2009) 1020.
[22] P.F. Carcia, R.S. McLean, M.H. Reilly, G. Nunes, Appl. Phys. Lett. 82 (2003) 1117.
[23] M.N. Kamalasanan, S. Chandra, Thin Solid Films 288 (1996) 112.
[24] W.J.E. Beek, M.M. Wienk, M. Kemerink, X.N. Yang, R.A.J. Janssen, J. Phys. Chem. B 109 (2005) 9505.
[25] D.C. Olson, Y.-J. Lee, M.S. White, N. Kopidakis, S.E. Shaheen, D.S. Ginley, J.A. Voigt, J.W.P. Hsu, J. Phys. Chem. C 112 (2008) 9544.
[26] C. Pacholski, A. Kornowski, H. Weller, Angew. Chem. Int. Ed. 41 (2002) 1188.
[27] B.Q. Sun, R.L. Peterson, H. Sirringhaus, K. Mori, J. Phys. Chem. C 111 (2007) 18831.
[28] W. Ma, C. Yang, X. Gong, K. Lee, A.J. Heeger, Adv. Funct. Mater. 15 (2005) 1617.
[29] D.C. Olson, Y.-J. Lee, M.S. White, N. Kopidakis, S.E. Shaheen, D.S. Ginley, J.A. Voigt, J.W.P. Hsu, J. Phys. Chem. C 111 (2007) 16640.
[30] K. Maturová, S.S. van Bavel, M.M. Wienk, R.A.J. Janssen, M. Kemerink, Nano Lett. 9 (2009) 3032.
[31] L.-M. Chen, Z. Xu, Z. Hong, Y. Yang, J. Mater. Chem. 20 (2010) 2575.
[32] S.-W. Cho, Y.T. Kim, W.H. Shim, S.-Y. Park, K.-D. Kim, H.O. Seo, N.K. Dey, J.-H. Lim, Y. Jeong, K.H. Lee, Y.D. Kim, D.C. Lim, Appl. Phys. Lett. 98 (2011) 023102.
[33] S. Yao, J. Appl. Phys. 50 (1979) 3390.
[34] J.C. Wang, X.C. Ren, S.Q. Shi, C.W. Leung, P.K.L. Chan, Org. Electron. 12 (2011) 880.
[35] M. Yun, R. Ravindran, M. Hossain, S. Gangopadhyay, U. Scherf, T. Bunnagel, F. Galbrecht, M. Arif, S. Guha, Appl. Phys. Lett. 89 (2006) 013506.
[36] C. Sah, L. Forbes, L. Rosier, A. Tasch Jr., Solid-State Electron. 13 (1970) 759.
[37] Z. Liu, M. Lo, H. Wang, T. Ng, V. Roy, C. Lee, S. Lee, Appl. Phys. Lett. 95 (2009) 093307.
[38] S.H. Park, J.G. Jeong, H.-J. Kim, S.-H. Park, M.-H. Cho, S.W. Cho, Y. Yi, M.Y. Heo, H. Sohn, Appl. Phys. Lett. 96 (2010) 013302.